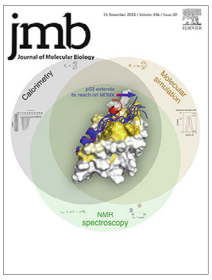

Vitis vinifera Lipoxygenase LoxA is an Allosteric Dimer Activated by Lipidic Surfaces

Stefania Pilati [1,*,‡], Klemens Wild [2,‡], Andrea Gumiero [2], Iris Holdermann [2], Yvonne Hackmann [2], Mauro Dalla Serra [3], Graziano Guella [4], Claudio Moser [1], and Irmgard Sinning [2,*]

*1 - **Research and Innovation Centre,** Fondazione Edmund Mach, Via E. Mach 1, 38098 San Michele all'Adige, Italy*
*2 - **Heidelberg University Biochemistry Center (BZH),** Im Neuenheimer Feld 328, 69120 Heidelberg, Germany*
*3 - **Institute of Biophysics,** CNR Unit at Trento, Via alla Cascata 56/C, 38123 Trento, Italy*
*4 - **Department of Physics,** University of Trento, Via Sommarive 14, 38123 Trento, Italy*

***Correspondence to Stefania Pilati and Irmgard Sinning:** stefania.pilati@fmach.it (S. Pilati), irmi.sinning@bzh.uni-heidelberg.de (I. Sinning)*
https://doi.org/10.1016/j.jmb.2024.168821
Edited by Georg Schulz

Abstract

Lipoxygenases catalyze the peroxidation of poly-unsaturated fatty acid chains either free or esterified in membrane lipids. *Vitis vinifera* LoxA is transcriptionally induced at ripening onset and localizes at the inner chloroplast membrane where it is responsible for galactolipid regiospecific mono- and di-peroxidation. Here we present a kinetic and structural characterization of LoxA. Our X-ray structures reveal a constitutive dimer with detergent induced conformational changes affecting substrate binding and catalysis. In a closed conformation, a LID domain prevents substrate access to the catalytic site by steric hindrance. Detergent addition above the CMC destabilizes the LID and opens the dimer with both catalytic sites accessible from the same surface framed by the PLAT domains. As a consequence, detergent molecules occupy allosteric sites in the PLAT/catalytic domain interface. These structural changes are mirrored by increased enzymatic activity and positive cooperativity when the substrate is provided in micelles. The ability to interact with micelles is lost upon dimer destabilization by site-directed mutagenesis as assessed by tryptophan fluorescence. Our data allow to propose a model for protein activation at the membrane, classifying LoxA as an interfacial enzyme acting on fatty acid chains directly from the membrane similar to mammalian 15-LOX and 5-LOX.

Introduction

Lipoxygenases (LOXs) catalyze the peroxidation of either free or esterified poly-unsaturated fatty acids (PUFAs) by the stereo- and regio-specific addition of molecular oxygen. Eukaryotic LOXs are characterized by a two-domain structure consisting of a PLAT (polycystin-1, lipoxygenase and alpha toxin) and a catalytic domain, whereas prokaryotic homologues lack a proper PLAT domain. Plant LOXs are divided into 9-, 13- and 9/13-LOX subgroups, according to the peroxidation site of their natural 18-carbon substrates linoleic and linolenic acid, and can have different optimal activity pH and subcellular localization (plastidial, cytosolic, or vacuolar).[1–3] Recently, an exhaustive phylogenetic analysis considering LOXs genes from 23 angiosperms proposed an evolutionary-based classification.[4] The high degree of diversification among LOX isoforms

reflects the ancient role of modifying membrane enzymes in stimuli perception and signal transduction. Diversification is further increased by specific gene expression profiles according to tissues and organs, developmental stages, and in response to environmental stresses. Main functional roles of LOXs[5] include the synthesis of (i) 9- and 13-HOTrE and HODE (from LnA and LA acid, respectively) representing the entry point of the oxylipin pathway that generates a wide variety of compounds involved in signaling[6,7]; (ii) C-6 volatile alcohols and aldehydes (also known as green leaf volatiles, GLVs) playing a role in plant defense, alerting neighboring plants of the presence of insects and fungal pathogens, and priming defense mechanisms[8]; (iii) C-5 volatiles and other volatiles (VOCs) considered flavors as they are appreciated by tomato consumers[9] or unappealing aromas as described for pea[10]; and (iv) phytoprostanes,[11] cyclopentenones,[12] jasmonic acid and smaller molecules such as azelaic and pimelic acids[13] as phytoalexins or signaling molecules involved in plant defense. Moreover, LOXs play a metabolic function related to lipid mobilization in seeds,[14] regulate plastidial physiological processes related to senescence[15] or morphogenesis,[16] and finally can be responsible for singlet oxygen ($^1O_2$) production as a signaling molecule.[17–21]

Vitis vinifera (*Vvi*, grapevine) LoxA is a 13-LOX induced at the onset of berry ripening[22,23] by the hormone abscisic acid.[24] This moment represents the irreversible transition from the vegetative/immature to the reproductive/mature developmental stage of the fruit, and it is characterized by a wide transcriptome reprogramming and deep cell metabolic and structural changes. In chloroplasts, the photosynthetic metabolism is switched off, requiring finely tuned plastid-nucleus communication and coordination to avoid metabolic impairment and reactive oxygen species accumulation. An initial characterization of LoxA showed its localization at the inner chloroplast membrane. Its ability to peroxidize membrane galactolipids, with the peculiarity to peroxidize both PUFA chains of each galactolipid molecule, was reported *in vivo* and confirmed *in vitro*.[23] Notably, a concomitant accumulation of $^1O_2$ was visualized inside chloroplasts at ripening onset.

From a structural point of view, plant LOXs consist of a single polypeptide chain with a molecular mass of 94–104 kDa including a N-terminal β-barrel PLAT domain and a larger catalytic domain containing a single non-heme iron atom.[5] In general, the PLAT domain is less conserved and is involved in protein-lipid or protein–protein interaction, whereas the α-helical catalytic domain shows a higher degree of structural conservation.[15,25] The catalytic site of known lipoxygenases is usually composed by the U or "boot" shaped cavity, with a defined depth to accommodate the substrate, the O_2 tunnel, and the substrate entrance site.[26] The LOX reaction proceeds through hydrogen abstraction from the sp^3 carbon of a pentadiene via a hydroxide that fills the metal coordination sphere (called $Fe^{III}(OH)$ cofactor).[27] The resulting free radical is delocalized along the pentadiene, and oxygenation occurs at the carbon ±2 from the site of attack. Hydrogen abstraction and oxygenation occur on opposite faces of the substrate, as shown in the structure of 8R-LOX with arachidonic acid.[26] The sidechains of the residues in the catalytic site influence the substrate preference, its "head–tail" orientation and the regio- and stereo-specificity of the O_2 addition. The substrate entrance site, which affects accessibility to the catalytic iron, is more variable among LOXs and difficult to predict as it is influenced by the overall structure of the protein. The structures of two bacterial LOXs, CspLox1 from *Cyanothece* and PaLox from *Pseudomonas aeruginosa*, missing the PLAT domain, showed that active site accessibility and orientation towards the membrane are determined by long N-term α-helices or β-barrel domains, which form a sort of lid over the entrance to the binding pocket.[25,28] Structural dynamics studies of soybean LOX implied a coupled thermal network within the catalytic domain shaping the active site[27] and of mammalian 15-LOX-2 identified the PLAT/catalytic interdomain contact as an additional region regulating substrate accessibility.[29]

Here, we present a detailed structural and kinetic characterization of *Vitis vinifera* LoxA based on crystal structures in a closed and an open conformation caused by the presence of detergent micelles, likely mimicking a lipid surface. Catalytic activity and cooperativity, affected by the presence of detergent micelles, rely on the stable dimeric form of the enzyme and suggest an interfacial mechanism of PUFA oxidation at the inner chloroplast membrane.

Materials and Methods

Cloning, expression, mutagenesis and purification of recombinant LoxA

Recombinant LoxA from grapevine (residues 48–901) was expressed and purified as described.[23] The double mutant (mLoxA) R787E:K869E was obtained by using the QuikChange Lightning site directed mutagenesis kit (Agilent Technologies). The double mutant was expressed and purified with the same protocol used for the wildtype protein. To remove imidazole, either a desalting step on a 5 mL-HiTrap column (GE Healthcare) or SEC on a Superdex 200 16/600 GL column (GE Healthcare) pre-equilibrated with 20 mM Hepes pH 8, 150 mM NaCl, and 1 mM β-mercaptoethanol were performed for both the wildtype and mutant protein.

Crystallization and data collection

LoxA samples were concentrated to 15 mg/mL. Diffraction-quality crystals of LoxA were grown in

sitting drops (250 nL protein + 250 nL reservoir) equilibrated at 18 °C against 100 μL reservoir containing 0.1 M Tris pH 9.2 and 22.5% (w/v) polyethylene glycol 4000. For co-crystallization attempts with detergents, 1 mM $C_{12}E_9$ (Anatrace) was added to the concentrated protein sample. Diffraction-quality crystals of LoxA in presence of $C_{12}E_9$ were also in sitting drops (200 nL protein + 100 nL reservoir) at 18 °C against reservoir containing 0.1 M Tris pH 9.2, and 26.4% (w/v) polyethylene glycol 4000.

All crystals were cryo-protected by a quick soak in reservoir supplemented with 25% (v/v) ethylene glycol immediately before snap cryo-cooling by plunging into liquid nitrogen. For crystals grown in the absence of $C_{12}E_9$, diffraction data were automatically recorded by Massif at 100 K at the European Synchrotron Radiation Facility (ESRF) beam line ID29 on a Pilatus_6M_F detector. Diffraction data for crystals obtained in the presence of $C_{12}E_9$ data were recorded at 100 K at the ESRF on beam line ID23-1 on a Pilatus_6M_F detector. All datasets were auto-processed by XIA2[30] and scaled and merged with AIMLESS.[31] Resolution cutoff was chosen by $<I/\sigma I> > 1$ and $CC_{1/2} > 0.5$.

Structure determination, refinement, and validation

Molecular replacement was performed in Phaser using a single molecule of soybean lipoxygenase-1 (PDB ID 4WFO) as a search model. A starting model for manual building was generated by Phenix[32] AutoBuild. Manual building was performed in COOT[33] using the structure provided by AutoBuild as a starting model. Refinement was performed in Phenix Refine in consultation with the validation statistics provided by COOT and MolProbity.[34] Molecular graphics were prepared using PyMOL (DeLano Scientific). Structure factors and final refined coordinates are deposited in the PDB. The structure of LoxA in the presence of $C_{12}E_9$ was solved using the apo structure as a search model, before continuing with model building as outlined above.

Small-angle X-ray scattering

SEC coupled to online SAXS was performed at the ESRF on beamline BM29. 100 μL of LoxA (20 mg/mL) were injected at 20 °C onto a Superdex 200 10/300 column (GE Healthcare) pre-equilibrated as stated above. Data was collected using the dedicated beamline software BsxCube and integration and buffer subtraction was performed on site. Data analysis was undertaken using the ATSAS software package[35]: twenty frames around the peak were averaged in Primus[36] and compared to theoretical scattering patterns from selected high-resolutions structures. The best fit was chosen based on the lowest Chi^2 value as given by Primus. *Ab initio* modeling was performed using the ATSAS web interface of Dammif,[37] selecting symmetric dimer as a restraint setting. The envelope model generated by Dammif was aligned to the closed LoxA structure and together visualized using PyMOL (DeLano Scientific).

Multi-angle light scattering

Multi-angle light scattering (MALS) experiments were performed by inline measurement of the static light scattering (DAWN 8+; Wyatt Technology) and the differential refractive index (Optilab T-rEX; Wyatt Technology) of protein samples separated on an S200 10/300 SEC column (GE Healthcare). For each run 100–300 μg of LoxA (native or mutant) were used. Data were analyzed using the ASTRA software package (Wyatt Technology).

Enzymatic activity assay

LoxA activity was measured spectrophotometrically by following the formation of the conjugated diene at 234 nm. Assays were performed at 25 °C in a final volume of 200 μL in 96-well UV-star plates (Greiner) using the plate reader Synergy2 (BioTek), using 1 μg of enzyme per assay (50 nM). Fatty acids (Sigma-Aldrich) were prepared using Tween20 according to Axelrod.[38] $C_{12}E_9$ or Tween20 (Sigma-Aldrich) were added at final concentration of 0.01% (v/v), unless other specified concentration. CMC for Tween20 was assumed to be 0.0074% (w/v) or 60 μM and for $C_{12}E_9$ 0.003% (w/v) or 50 μM .[39] For the pH dependence study, 0.1 M MES buffer was used for pH 5–7 and 100 μM linolenic acid (LnA). The first order initial kinetic rates were estimated by linear fitting of absorbance measured at 234 nm per sec within the first 0–30 sec and converted into (μmol min^{-1} mg^{-1}), using an extinction coefficient ε = 23,000 M^{-1} cm^{-1} for the conjugated double bond of peroxidized LnA and a MW (LoxA) of 98 KDa. All statistical analyses have been done using R.[40] LoxA and mLoxA velocity vs. substrate concentration were fitted using Eqs. (1) and (2), respectively:

$$V = (Vmax * S^n)/(K^n + S^n) \quad (1)$$

$$V = (Vmax * S)/(KM + S) \quad (2)$$

Lipid analysis in mass spectrometry

The reaction products as formed by the incubatiion of wildtype and mutant mLoxA with linoleic acid (LA, 18:2), linolenic acid (α18:3 and γ18:3), and 20:3 (Sigma-Aldrich) and mutant mLoxA with α18:3 have been assayed by HPLC-MS/MS as previously described.[23]

Trp fluorescence measurements

Tryptophan fluorescence of wildtype and mLoxA was measured with a Fluoromax 4 (Horiba Scientific), setting excitation wavelength at 295 nm and recording light emission in the range 300–450 nm, with a 1 nm scan and 2 nm slit width. Protein concentration was 250 nM in each assay. For each pH buffer, either $C_{12}E_9$ or Tween20 was added at 0.01% (w/v) and after 5 min fluorescence was measured again. DeltaF/F was calculated as the difference in fluorescence before and after detergent addition (corrected for protein dilution) normalized on the initial value.

Size exclusion chromatography

Oligomeric state determination of wildtype and mLoxA was performed by SEC using a Superdex200 Increase 10/300 GL column on AKTA Purifier (Cytiva) pre-equilibrated with 20 mM HEPES pH 7.5, 150 mM NaCl, and 0.01% (v/v) $C_{12}E_9$ when specified. The apparent molecular mass was estimated using a calibration curve of a mix of protein standards (LMW and HMW Gel Filtration Calibration Kits, Cytiva) covering from 6.5 to 440 kDa.

Inductively coupled plasma (ICP) atomic emission spectroscopy

Two different preparations of LoxA and mLoxA, respectively, were diluted 10 times with ultrapure water to lower HEPES and NaCl concentrations and then concentrated to 4–10 mg/mL using Amicon ultracentrifugal filters (30 KDa cut-off; Merck). Samples (150 μL) were incubated with an equal volume of ultrapure nitric acid at 70 °C for 1 h and then diluted to 3 mL with pure water. Iron and Manganese quantification was performed with an inductively coupled plasma-mass spectrometer in 'He mode' (ICP-MS 7800, Agilent technologies). The instrument was calibrated against external certified standard solutions of Fe and Mn and repeatability of duplicate analysis was below 5%. Blank buffer samples, prepared together with protein samples, were measured in the same analytical batch.

Accesion numbers

PDB: 8QDQ, 8QDR.

Results

LoxA is a dimeric lipoxygenase

For structural and functional analyses, recombinant LoxA protein from grapevine was expressed in *Escherichia coli* and purified as described.[23] The purification scheme was extended by a size exclusion chromatography (SEC) step coupled to multiangle light scattering (MALS) for molecular weight analysis and increased purity necessary for subsequent crystallization. Although most characterized LOX enzymes act as monomers or only transiently form dimers,[41] LoxA (MW of 96.3 Da) purified as stable homodimer (Figure 1a). Dimer containing fractions were pooled, concentrated to 15 mg/mL and subjected to crystallization. Monoclinic crystals grew in PEG conditions and data could be collected to 2.0 Å resolution at the European Synchrotron Radiation Facility (ESRF) (Suppl. Table 1). The structure of LoxA was solved by Molecular Replacement using soybean lipoxygenase-1 (PDB ID code 4WFO) as a search model. The structure reveals two molecules per asymmetric unit with a tight and extended interface. The interface analysis by the PISA server[42] confirmed the formation of a stable dimer with an interface area of 1,900 Å^2.

In order to validate that the dimer observed in solution by MALS and in the crystal structure share the same interface, we performed SEC coupled to inline small-angle X-ray scattering (SAXS). For analysis, we aligned the experimental scattering curve of LoxA to theoretical scattering curves calculated based on the LoxA monomer

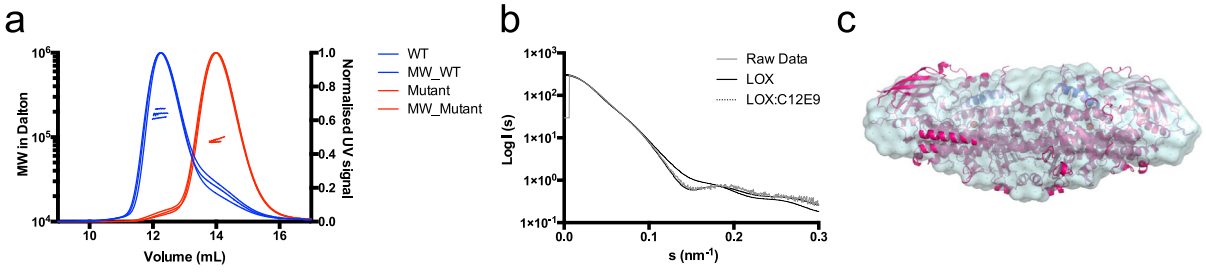

Figure 1. MALS and SAXS analyses of LoxA. (a) Normalized SEC elution profiles and MALS analyses. Native LoxA (blue trace) purified as a homodimer. A double mutation in the dimerization interface induces the monomeric form (red trace) as explained below. MALS analyses were done in triplicates and the molecular weight traces are given for the peaks within the elution profiles. **(b)** Solution scattering traces of LoxA and LoxA accommodating $C_{12}E_9$ (co-crystallization experiments explained later) fitted to SAXS data. The best fit was statistically evaluated by the lowest Chi^2 values. **(c)** *Ab initio* model and molecular envelope fitted to the LoxA dimer.

and dimer and other LOX structures, and statistically evaluated the fit by comparison of Chi^2 values (Figure 1b, Suppl. Table 2). The best fit matched the dimeric LoxA structure. Using the scattering data, we created an *ab initio* model and a molecular envelope, which we then fitted onto our dimeric structure (Figure 1c). Again, the shape of the molecular envelope showed an excellent overlap with the crystal structure of LoxA thus confirming the relevance of the observed crystallographic dimer.

Structure of the LoxA dimer

Like all plant lipoxygenases, grapevine LoxA consists of a N-terminal PLAT domain and a C-terminal catalytic domain. The catalytic domain is responsible for symmetric homodimerization thus creating an extended flat surface including the peripheral PLAT domains, and an opposite surface with convex shape (Figure 2a). The active sites harboring the catalytic irons are deeply buried within the dimer structure. The PLAT domain fold, which has been comprehensively analyzed,[43,44] comprises a β-sandwich composed of two sheets made up from four anti-parallel β-strands (residues 67–204) (Figure 2a and Suppl. Figure 1). In LoxA, strand connections are well ordered except for the β1-β2 loop (residues 79–104) that includes two flexibly linked α-helices. This domain is found in a variety of membrane or lipid associated proteins and is known to be involved in membrane attachment via the exposure of hydrophobic residues and Ca^{2+} binding,[45] although sequence homology is low.[43] The PLAT domain is connected via a short linker to the more conserved and mostly α-helical catalytic domain (core of 17 helices and two β-sheets, 23 helices in plants,[46] residues 217–901) housing the non-heme iron center. Typical for plant lipoxygenases, LoxA contains several insertions to the common core (Suppl. Figure 1). Due to an extended insertion C-terminal to helix α2, this functionally important helix is tilted like in all plant LOXs in regard to the animal or bacterial enzymes and occludes access to the catalytic site.[47] The insertion together with helix α2 and flanking regions form a lid-like structure (LID, residues 306–396) comprising three more α-helices and a three-stranded antiparallel β-sheet (Figure 2a and Suppl. Figure 1). Together with the PLAT domain, the LID is the most flexible part of the structure as inferred from temperature factor analyses (Suppl. Figure 2). Thus, flexibility is pronounced on the flat side of the dimer above the active sites. According to the isoelectric point of 5.6, the overall electrostatic surface potential of the dimer is rather negative, with charged patches clustering next the domain interfaces (Figure 2b).

Apart from the LID, plant-specific LoxA insertions in respect to the common fold of the catalytic domain are clustered at the dimer interface and increase the contact surface (Figure 2c and Suppl. Figure 2). Most prominent, at the lateral sides of the interface a three-turn α-helix (α19 in plants) is in tight contact *in trans* with the LID and the C-terminal loop, which is also extended. More central in the interface, the N-terminus of the longest helix α9 is elongated by one turn (531–534) towards the interface and two tryptophans (W531, W537) are exposed into the interface. At the center of the symmetric dimer, three aromatic residues (F397, W399, F400), following the LID, cluster with their respective partners. Overall, the interface is hydrophobic at the center and at the periphery reveals an extensive hydrogen bonding network and four salt bridges (R787:E864 and E532:K869, respectively).

The intramolecular PLAT/catalytic domain contact and orientation are the same as found in all lipoxygenases due to the conservation of a central π-cation bridge (W189-R301) (Figure 2d).[48] The arginine is spanned by salt-bridges in between E166 of the PLAT and D307 in the beginning of the LID domain. LoxA-specific, the β1-β2 loop of the PLAT domain exposes an α-helix that forms a hydrophobic helix-bundle with helices α2 and α3 of the LID domain. The internal β1-β2 loop structure is further stabilized by tryptophan W100 stacking on top of valine V80 and being backed by a hydrogen-bond network involving two histidines (H163, H164).

The boot-shaped active site

The conserved catalytic core of lipoxygenases is also present in LoxA. It harbors a non-heme iron pseudo-octahedrally coordinated by three histidine residues (H559, H564, H751), provided by π-helical segments within the two longest helices α9 and α18, an asparagine side chain (N755, weakly coordinated), and the carboxyl of the C-terminal isoleucine (I901) (Figure 2e). The 6th coordination position of the iron is occupied by a water molecule (or hydroxide)[49] and faces the boot-shaped substrate-binding pocket as found in all lipoxygenases (more U-shaped in bacteria and mammals.[26] The hydrophobic pocket is lined by a universal 'arched' helix (helices α11 and α12) with an internal three residue hairpin (residues 608–610). Aliphatic substrates bend around an invariant leucine at the arch (L606) and substrate regio-specificity is determined by variation of the depth of the pocket. For LoxA, phenylalanine F617 at the C-terminus of the arched helix limits the pocket size as known to be necessary for 13-LOX activity.[50] S-LOX stereochemistry of the reaction is determined by an alanine (A602 in LoxA, termed 'Coffa-site') within the arched helix, which is exchanged for a glycine in R-LOXs enzymes.[51] In the LoxA structure, substrate entry is blocked by a leucine gate (or 'cork')[47] formed by two leucines of helix α2 (L318, and L322 within a conserved π-helical turn), and the invariant L606 of the arched

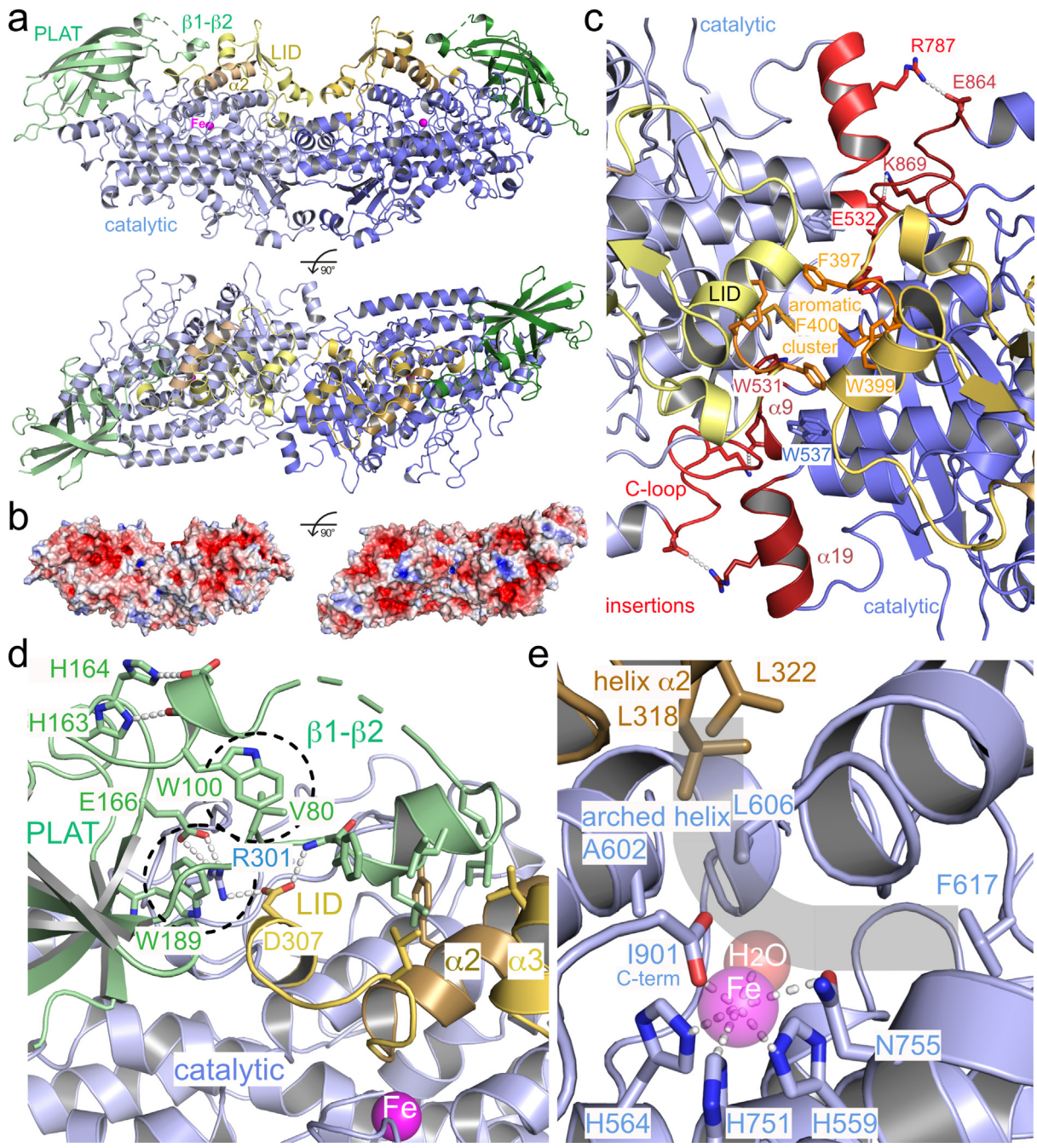

Figure 2. The LoxA dimer structure. (a) Overall structure of the LoxA dimer and domain architecture. The catalytic iron ions are deeply buried below the LID including helix α2. **(b)** Electrostatic surface potential (±5 kT) in the same views. **(c)** The dimer interface along the symmetry axis. Dimer relevant insertions are given in red tones and prominent residues and salt bridges are labelled. **(d)** The PLAT-catalytic domain contact. Tryptophan mediated contacts are encircled and connected hydrogen-bond networks indicated. The β1–β2 loop is fixed on helices α2 and α3 of the LID by hydrophobic interactions. **(e)** The catalytic site of a LoxA subunit. The coordination sphere of the iron is detailed. The boot-shaped substrate-binding pocket (outlined in gray) is closed by helix α2. Important residues within the pocket are given.

helix. LoxA therefore adopts a closed conformation as previously described for other Loxs.[47,52]

To prove the structural findings, reaction specificity was assayed by incubating LoxA with different substrates, such as alpha-linolenic acid (18:3, n-3), linoleic acid (18:2, n-6), gamma-linolenic acid (18:3, n-6), and eicosatrienoic acid (20:3, n-6), all differing in number and position of the double bonds and chain length. Analysis of the reaction products by HPLC-MS/MS revealed that

the far most prevalent product was peroxidized on C-13 for 18C substrates and on C-15 for the 20C substrate. These results indicated that C-11 (or C-13 for 20:3) is always positioned in front of the iron and that the active site cannot accommodate longer tails in agreement with the presence of F617 limiting the size of the boot-shaped substrate-binding pocket (Figure 3).

The LoxA open conformation

As the substrate-binding pocket is blocked by the LID within our dimeric LoxA structure, we wondered how to achieve a substrate-bound complex. We tried to co-crystallize LoxA in the presence of natural galactolipid substrates, however, without success. Since LoxA functions at the inner chloroplast membrane, we then tried co-

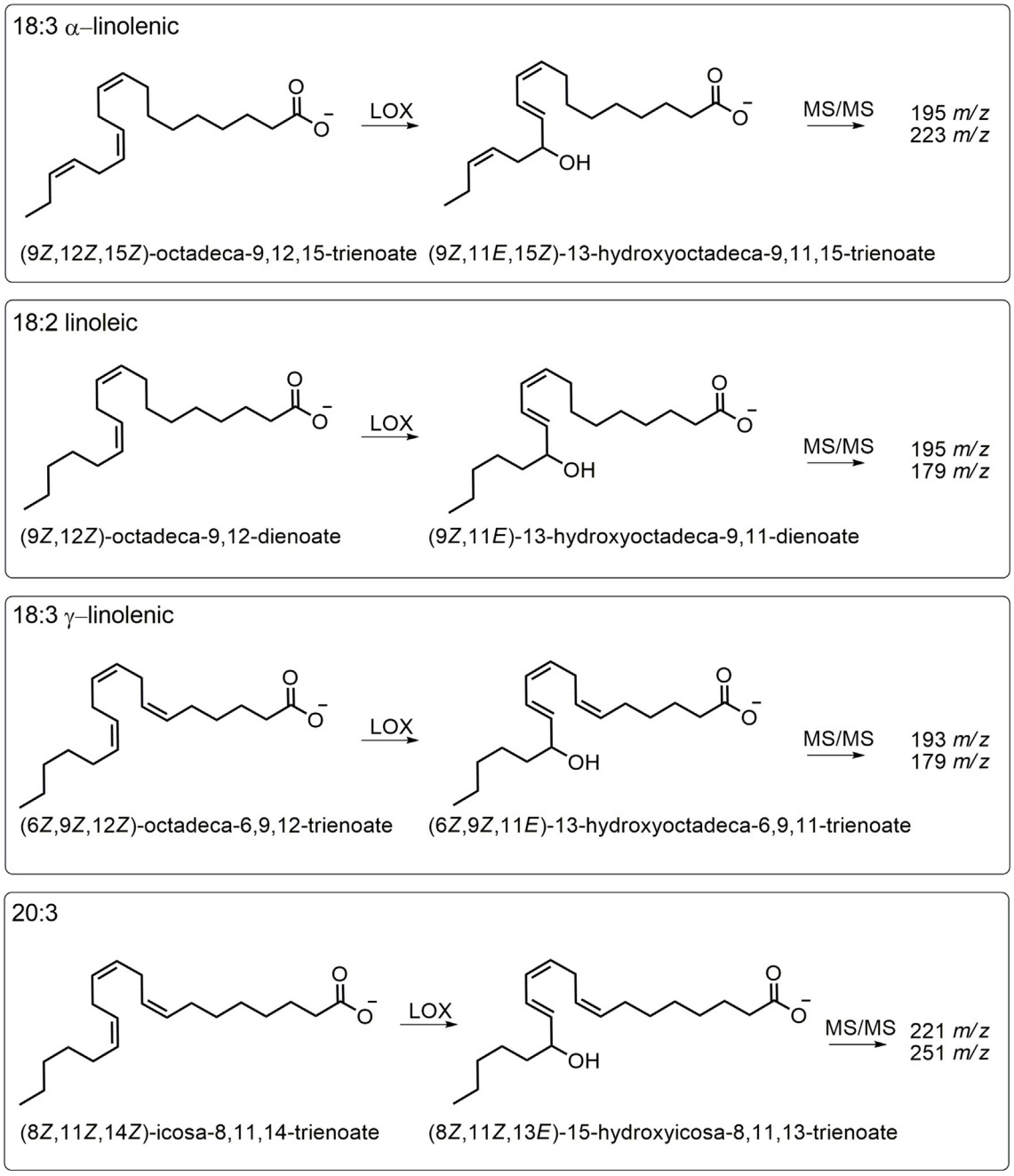

Figure 3. PUFA peroxidation by LoxA. LoxA was incubated with four different substrates. α- and γ-linolenic acid (18:3, ω-3 and ω-6) reacted to 13-hydroxyoctadecatrienoic acid (13-HOTrE), linoleic acid to 13-hydroxyoctadecadienoic acid (13-HODE), and eicosatrienoic acid to 15-hydroxyeicosatrienoic acid (15-HETrE). MS/MS diagnostic fragments identifying the products are reported on the right.

crystallisation with mild detergents that would mimic the membrane environment and could potentially alter the structure to accommodate substrate. Indeed, we were able to obtain crystals of LoxA together with the detergent $C_{12}E_9$ used at a concentration above the critical micellar concentration (CMC). Crystals were non-isomorphous to the previous LoxA crystals but again contained two molecules per asymmetric unit. They diffracted as well to 2.0 Å and the structure was solved by Molecular Replacement using the closed LoxA structure as template (Suppl. Table 1). LoxA was found to form the same dimer (rmsd of 0.68 Å), but electron density was absent for extensive regions, which included the LID, presumably due to an increase in mobility invoked by the presence of detergent micelles (LID boundaries defined according to the melting) (Figure 4a and Suppl. Figure 3). Interestingly, the LID includes a region implied in a coupled thermal network within the catalytic domain as observed by temperature-dependent hydrogen deuterium exchange (TDHDX) for soybean LOX-1[27] (Suppl. Figure 4). In this study, the authors suggest that distal protein motions could be directly linked to the activation of hydrogen tunneling in the active site. Moreover for LoxA, although the crystallographic space group had changed, the same arrangement for a dimer of dimers was observed, established via the antiparallel alignment of the C-terminal helices α22 (Suppl. Figure 5). Interestingly, while the PLAT domain seemed to be stabilized in the open conformation according to temperature factor analyses, the region around the solvent exposed active site became highly flexible (Suppl. Figure 2). Moreover, this region now formed a highly negatively charged surface patch (Figure 4b). The effect of detergent was also studied in solution by SEC, where a reduction of aggregation in favor of the dimer was observed (Suppl. Figure 6).

Although the overall dimer interface in the open conformation is the same as before, significant structural changes can be detected. LID melting is communicated to the adjacent aromatic cluster at the interface, which is retracted from the center of the interface (Figure 4c) leaving a large water filled void. Thus, the size of the interface shrinks by 600–1300 Å^2. Similarly, LID melting destroys the extended tertiary contact to the β1-β2 loop of the PLAT domain (Figure 4d) (interface reduction from 1350 to 950 Å^2, ΔG < 50%) and the helix bundle observed in the closed conformation is completely dissolved. While the domain arrangement remains unaltered due to the maintained π-cation bridge (W189-R301), the release of the β1-β2 loop remodels the surface of the PLAT domain on top of the β-sandwich. Most strikingly, W100 swaps from its internal position in the interface (closed conformation, Figure 2d) by 19 Å to the top of the PLAT β-barrel (Figure 4d).

Most importantly, the melting of the entire LID grants access to the substrate-binding pocket while leaving the active site including iron coordination intact (Figure 4e). Melting of the LID including the displacement of helix α2 (Suppl. Figure 3), and the partial melting of the penultimate helix α21, opens the leucine gate as observed in the closed structure and would allow the substrate to enter the pocket. While we do not observe any detergent bound in the substrate-binding pocket, an ethylene glycol molecule introduced for cryo-protection of the crystals now occupies the 6th position of the iron coordination. In addition, N755 is retracted from the iron due to LID removal and unexplained difference density is found towards the iron, which could correspond to a second water molecule coordinated to the iron as suggested by EPR studies on soybean LOX-1.[53]

In addition to changes in the active site, the melting of areas close to the C-terminus (residues 816–823 and 887–893) opens an additional binding pocket for a partially hydrophobic moiety, which is filled by a $C_{12}E_9$ molecule stabilized by several hydrogen-bonds (H591, W685, H830) (Figure 5). Opening occurs via a change of side-chain conformation of tyrosine Y897 induced by local structural rearrangements and including a relay system (Y897-R593-Y594-E825). The pocket locates to the PLAT domain interface and is too far from the active site to be part of the substrate-binding pocket. Interestingly, it has been previously characterized as allosteric site for 13-HODE binding to human epithelial 15-lipoxygenase-2.[54] There, pH-dependent allostery was attributed to three residues also being mainly involved in ligand binding in LoxA (H830, R593, Y594). The PLAT domain mediated allostery has been comprehensively annotated as general mechanism in plant and animal lipoxygenases.[44] Our data indicate that this allosteric site and mechanism is present also in our LoxA.

A double mutation destabilizes the LoxA dimer and abrogates its interaction with lipidic surfaces

The closed and open conformations of LoxA highlight four conserved salt bridges at the dimer interface, R787:E864 and E532:K869, respectively. To better understand the implication of the dimeric nature of LoxA, so far only observed for mammalian 12/15-LOX,[41] we produced a double mutant, in which the salt bridges were replaced by repelling charge pairs (R787E and K869E) in order to destabilize the dimer. Notably, these four residues are not conserved among the plant Loxs belonging to the same phylogenetic group[23] and the human Lox15B considered for the alignment of Suppl. Figure 2. We expressed and purified the mutant protein (mLoxA) following the

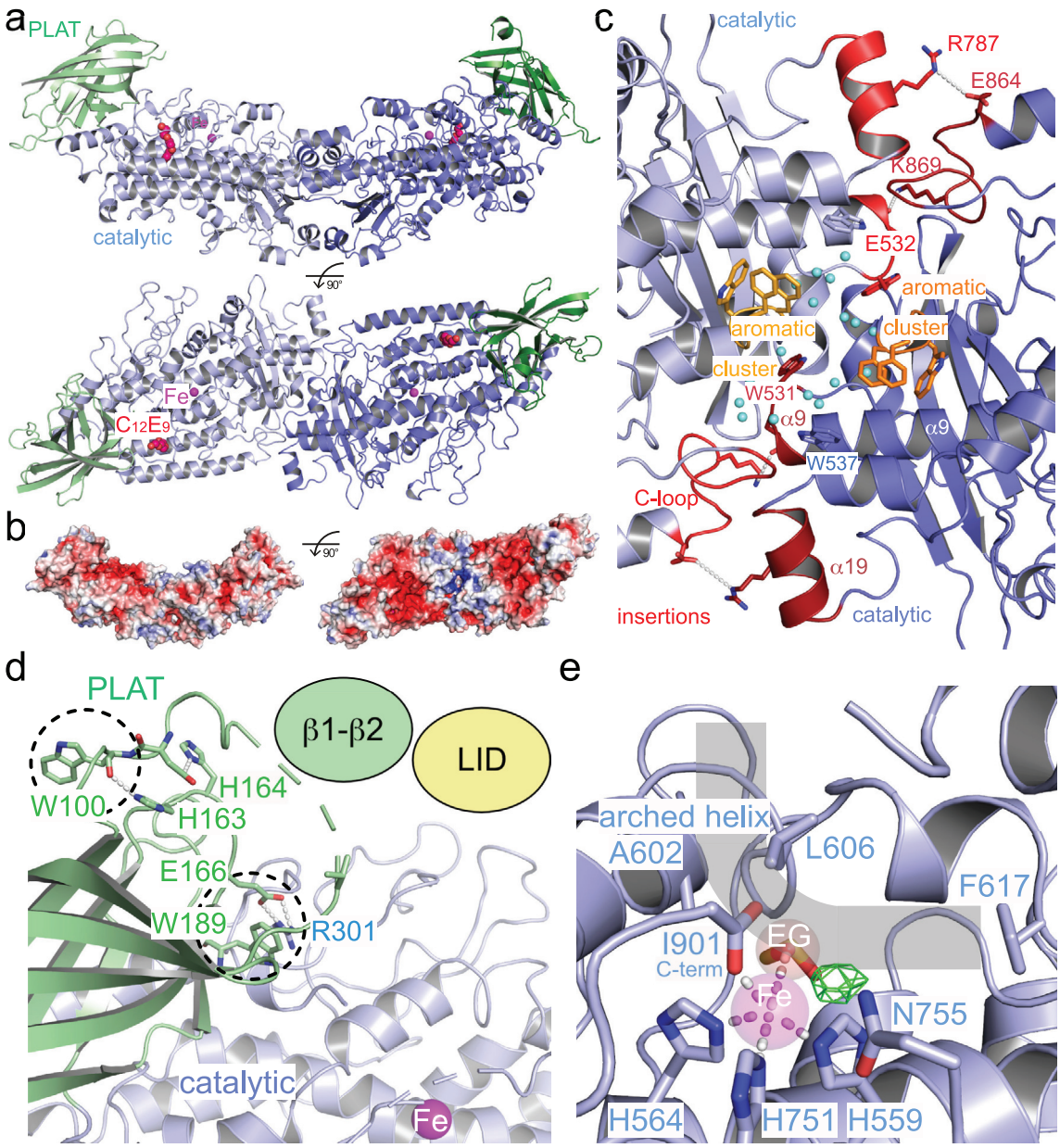

Figure 4. The open LoxA-$C_{12}E_9$ structure. (a) Overall views of the open LoxA dimer. The LID domains are completely dissolved. The catalytic iron ions (pink) are now solvent accessible. Detergent molecules (red) fill cavities at the PLAT/catalytic domain interface. **(b)** Electrostatic surface potential (±5 kT) in the same views. **(c)** The dimer interface around the symmetry axis. The aromatic clusters in the center of the interface are separated and water molecules (cyan spheres) fill the void. **(d)** The PLAT/catalytic domain contact. Compared to closed LoxA, the W189 mediated contact remains, while W100 flips to the PLAT domain surface (encircled). The β1-β2 loop and LID domains are dissolved, and the hydrophobic contact is broken. **(e)** The catalytic site of a LoxA subunit. The boot-shaped substrate-binding pocket (outlined in gray) is open as helix α2 is gone. An ethylene glycol (EG) molecule occupies the position of the catalytic water (or hydroxide, position outlined by a red sphere). N755 retracts due to LID removal and unexplained difference density (4.5 σ, green) is found towards the iron.

same protocol used for the wildtype protein. Performing SEC of mLoxA, we observed that it eluted predominantly as monomeric protein (Figure 1a). Both wild-type and mutant LoxA metal binding were analyzed by ICP atomic emission spectroscopy, indicating that both proteins specifically bind iron. Semi-quantitative analysis of the metal to protein monomer ratio indicated an overall higher proportion for the wild-type compared to the mutant.

Tryptophan fluorescence was used to investigate lipid interaction of wildtype and mutant LoxA, mimicked by the addition of detergent micelles

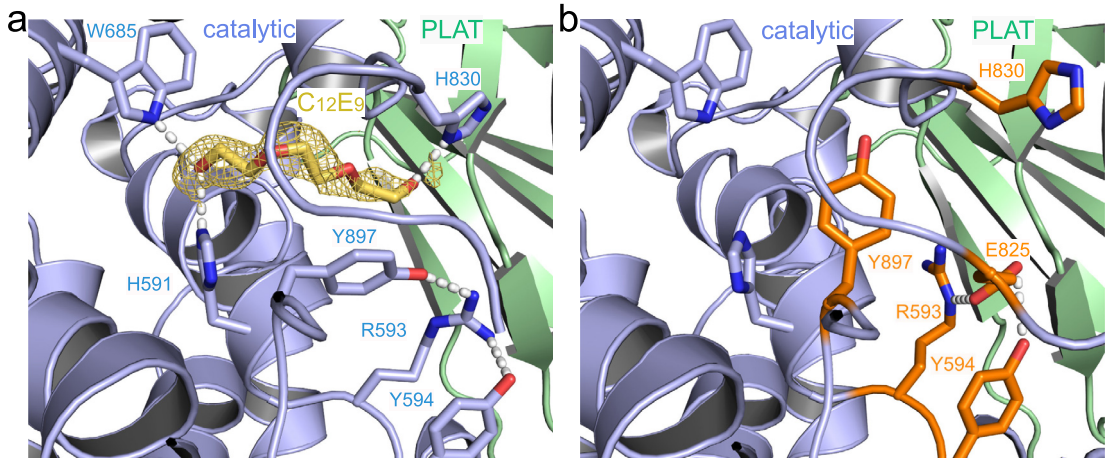

Figure 5. Allosteric site in the PLAT/catalytic domain interface. (a) A $C_{12}E_9$ molecule in the allosteric site of the open LoxA structure. The detergent (yellow, only partially visible) is covered with its 2*m*Fo-*D*Fc map contoured at 0.8 σ (yellow). Hydrogen-bonding side-chains in the site are given. Tyrosine Y897 lining the site is part of an ordered relay with R593 and Y594. **(b)** The allosteric site is closed in the closed LoxA structure. Rearranging residues are given in orange. Without ligand present, the relay relaxes towards the void and is stabilized by glutamate E825. Histidine H830 swings out of the site.

(Figure 6). In the case of the wildtype protein, an increase of tryptophan fluorescence intensity was recorded upon detergent addition, while the emission spectra of mLoxA remained unchanged. The emission maximum (342 nm) remained almost invariant, suggesting that the microenvironment polarity was not significantly affected, thus excluding that tryptophans change their solvent exposure. This result indicates that a local structural change in a region including one or a few tryptophan residues occurred upon lipid interaction in the wildtype dimer, while it was not detectable in the monomeric mutant. For the wildtype protein also pH 6 and pH 7 were tested revealing that the increase in tryptophan emission occurred only at pH 6.5 and pH 7, while at pH 6 it was decreasing. Thus, a coordinated tryptophan/histidine movement can be envisioned. The crystallographic analysis showed that the addition of the detergent $C_{12}E_9$ during LoxA crystallization resulted in conformational changes mainly involving the LID domain and its PLAT interface, the allosteric pocket, and the dimerization interface, all of them including one or more

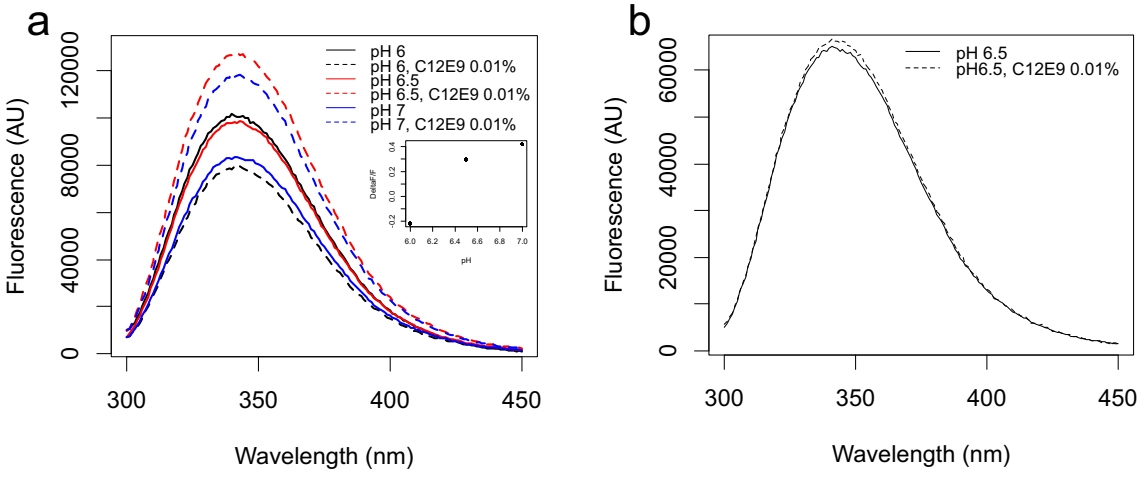

Figure 6. Tryptophan fluorescence emission spectra of wildtype and mutant LoxA in the presence of detergent micelles. (a) Wildtype LoxA emission spectra were recorded at the indicated pH-values before and after the addition of the detergent $C_{12}E_9$ (final concentration 0.01% (v/v)). In the inset, the relative variation of fluorescence at each pH value is represented. **(b)** mLoxA emission spectrum recorded at pH 6.5 before and after addition of the detergent as in a). Excitation wavelength was 295 nm in all experiments.

tryptophan and histidine residues (Figures 2 and 4). Due to structural rearrangements in the PLAT domain, tryptophan W100 stabilizes the β1-β2 loop contacting the LID in the closed conformation and is swapped onto the protein surface of the open conformation in a guided movement supported by two histidine residues (H163, H164) stabilizing the protein backbone. Similarly, the $C_{12}E_9$ binding pocket involves two tryptophans (W685, W835) and two histidines (H591, H830), and the dimer interface involves three tryptophans (W399, W531, W537) and histidine H791. Notably, for all of them the environment changes upon detergent binding. Thus, all these changes and the central involvement of histidine residues might result in a pH-dependent fluorescence change when measured in solution.

Enzymatic activity of LoxA and its monomeric mutant

Kinetic analyses of the wildtype dimer and monomeric mutant were carried out to explore the effects of the lipid presence and pH condition on the enzyme functionality and properties. Preliminary assays highlighted that LoxA enzymatic activity was improved in terms of measurement stability and reproducibility by adding either $C_{12}E_9$ (the detergent used for crystallization) or Tween20 (the detergent used for fatty acid preparation) at concentrations above their CMC (not shown). These results indicated that the conformational changes induced by the presence of detergent positively affects its catalytic properties, even if we cannot exclude another contribution derived from the way the substrate is presented. Therefore, detergent was always added to the reaction mix for the wildtype protein. Conversely, mutant activity was not affected by detergents (not shown), which was added only to improve substrate solubility at high concentrations. Based on previous literature,[55] the pH-dependence of enzyme activity was tested in the pH range 5 to 7 (Figure 7a). For LoxA, maximum activity was measured at pH 6.4 with a sharp decrease on the basic side and some residual activity still present on the acidic side up to pH 5 that did not allow to fit data with a bell-shaped curve. Remarkably, mLoxA showed maximal activity at pH 5, although about 13 times lower than that of the wildtype protein (Figure 7b). However, as observed for LoxA, activity was completely lost at pH higher than 6.5. Product formation was verified by HPLC-MS analysis, confirming the decrease in efficiency and also specificity of linolenic acid peroxidation (Suppl. Figure 7).

To gain more insights into the pH influence on LoxA catalysis, kinetic studies at optimal pH and pH 5 were carried out. At the optimal pH 6.4, a sigmoidal increase of the initial rate was obtained (Figure 8a), revealing the cooperative behavior of the enzyme as confirmed by Hill plot transformation analysis (cooperativity index, n = 2.6) (Suppl. Figure 8). Quite surprisingly, at pH 5 LoxA showed a Michaelis-Menten behavior characterized by a hyperbolic curve (Figure 8b). As previously observed by Trp fluorescence, LoxA conformational changes occurred above pH 6, which might be a requirement for cooperative behavior. Kinetic analysis of the mutant at its optimal pH 5 showed a hyperbolic trend as expected for monomeric enzymes (Figure 8c). The lower Fe-binding ability of the mutant can partially explain the lower activity, but the loss of cooperativity is likely due to the loss of the dimeric structure. Kinetic parameters calculated from fitting the experimental data are shown in Table 1 (see Suppl. Figure 9 for statistical analyses). From these analyses, we conclude that the catalytic unit of LoxA is the dimer, characterized by cooperative

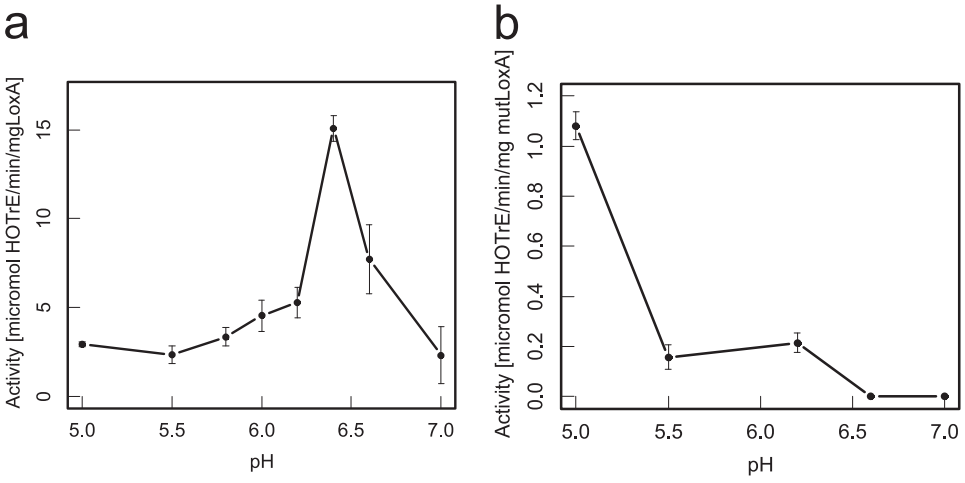

Figure 7. pH-dependence of wildtype and mutant Loxa activity. (a) Wildtype LoxA and **(b)** monomeric mutant LoxA activity measured in the presence of 0.01% (v/v) Tween20 and 100 μM linolenic acid as substrate. Technical replicates and standard deviation are shown (n = 3).

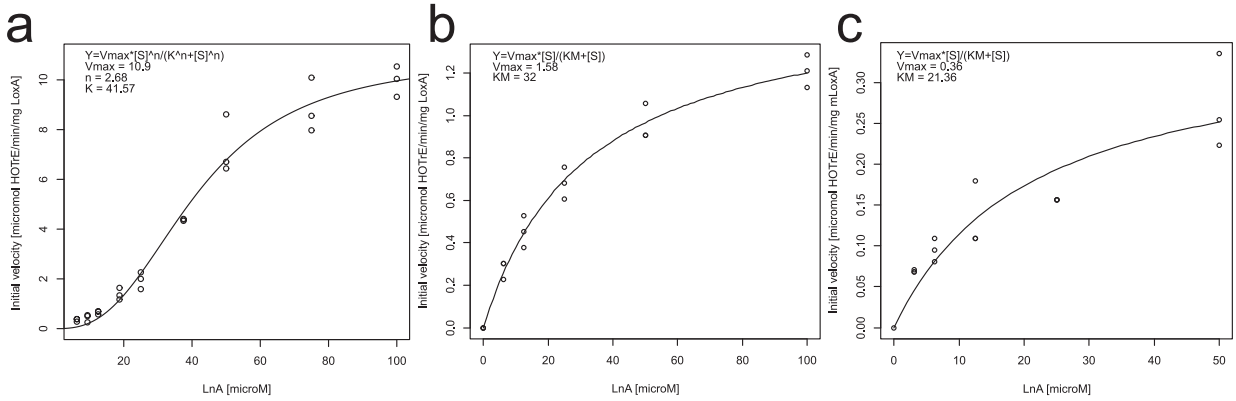

Figure 8. Kinetic profiles of wildtype LoxA. (a) LoxA activity assays were performed at pH 6.4. **(b)** Wildtype LoxA and **(c)** mutant mLoxA activity assays were performed at pH 5. The solid line represents the best fit obtained by nonlinear regression of the data using the indicated equation. All experiments were performed in 0.1 M MES and 0.01% (v/v) Tween20.

Table 1 LoxA kinetic characterization.

	pH	v_{max} (μmol min^{-1} mg^{-1})	K_M or $K_{1/2}$ (μM)	k_{cat}* (sec^{-1})	Type of kinetics	Influence of detergent on structure and catalysis
LoxA	6.4	10.9 ± 0.6	41.6 ± 2.7	18.2 (36.4)	Positive cooperativity	Yes
LoxA	5.0	1.58 ± 0.08	32.0 ± 3.8	2.6 (5.2)	Michaelis-Menten	No
mLoxA	5.0	0.36 ± 0.06	21.3 ± 8.0	0.6	Michaelis-Menten	No

* For k_{cat} calculation, the molarity of the monomer was used. k_{cat} calculations considering the dimer are reported in parenthesis. LoxA denotes the wildtype enzyme, "m" its monomeric mutant as specified in the text.

kinetics occurring within a narrow pH interval around pH 6.4.

To further investigate the influence of detergent on LoxA activity, we performed assays at two detergent concentrations (0.01% and 0.02% (v/v) Tween20) with the same substrate concentration and then at increasing substrate and detergent concentrations, albeit keeping their molar ratio constant. We observed that the cooperative behavior was maintained, but the two sigmoidal curves were shifted, resembling a dilution effect of the detergent on the substrate (Suppl. Figure 10, a–b). Plotting initial velocity vs the ratio [LnA]/[Tween20], the two curves overlapped, indicating that this ratio was a relevant parameter and that above a certain threshold activity decreased due to substrate solubility and/or unfavorable partitioning among bulk and micelles. V_{max} was reached at 125 μM linolenic acid in Tween20 0.01% (v/v) and 175 μM in Tween20 0.02% (v/v), but for the same ratio (1.2–1.5 in the tested conditions). To better estimate the saturating substrate concentration, keeping in mind that LoxA localizes at the inner chloroplast membrane where poly-unsaturated galactolipids are extremely abundant, we increased the linolenic acid concentration up to 0.5 mM, but keeping the optimal [LnA]/[Tween20] ratio between 1.2 and 1.9. Notably, LoxA was not inhibited at such high detergent concentrations, and V_{max} was confirmed to be around 10.9 ± 0.6 μmol/min/mg for a ratio around 1.8, which likely corresponds to a substrate per area density rather than bulk concentration (Suppl. Figure 10, c–d).

Taken together, characterization of the LoxA enzymatic activity showed that detergent impacts on both enzyme and substrate. Linolenic acid solubilization in detergent micelles mimicks membrane galactolipids esterified fatty acid chains and triggers the transition from the closed to open LoxA conformation, which allows for positive cooperativity.

Discussion

We report the structure and enzymatic characterization of the constitutive dimeric plant lipoxygenase LoxA from grapevine. *In vivo*, LoxA has been localized inside the chloroplast, tightly associated to the inner membrane where it catalyzes the peroxidation of galactolipid PUFA chains[23]. The connection between oligomerization state, membrane binding and catalytic properties has been deeply investigated for human LOXs, such as h12-LOX and h15-LOX-2,[41,56,57] and recently also by structural methods such as hydrogen–deuterium exchange and cryo-electron microscopy.[58,59] In the present work, we solved the crystal structures of the protein without and in the presence of the detergent $C_{12}E_9$ (above

CMC), while complexes with its natural substrates (the galactolipids) could not be obtained. The protein-detergent interaction and its impact on protein structure and activity likely mimicking lipid membrane binding, was confirmed by tryptophan fluorescence and kinetic analyses, and its dependence on LoxA dimerization was verified by comparison with a monomeric mutant.

The LoxA dimer, confirmed in solution by SEC-MALS and SAXS data, showed a symmetric orientation with the N-terminal PLAT domains located at the sides. So far, only rabbit reticulocyte ALOX15 was crystallized in a dimeric form,[56,60] where dimerization relied on a contact between the lateral helix α2 of the catalytic domain of the two monomers and was transiently induced by the binding of an inhibitor. Also structural studies conducted on hLOX12 reported a dimeric form,[58,59] which relied on the hydrophobic interaction between leucine and aromatic residues exposed on helix α2 of each monomer. The LoxA dimerization interface is much more extended (1,900 $Å^2$), involving helices α9 and α19, enriched in aromatic residues at the center and stabilized by a surrounding extensive hydrogen bonding network and salt bridges. Higher oligomerization states for LoxA are possible, reported also for hLOX12,[59] as helix α22-mediated lateral tetramerization is observed in the crystal packing. Dimer formation positions the two active sites harboring the Fe^{3+}-ions on the same side suggesting that *in vivo* this surface interacts with the membrane. In contrast to the closed conformation, in the presence of detergent micelles this surface shows higher flexibility compared to the PLAT domains, which seem stabilized. This binding mode is a typical feature of interfacial enzymes, which need to bind to membranes for accessing their substrates avoiding their solvent exposure as described for phospholipase A2.[61,62] This mechanism agrees with the observed association of LoxA to the inner chloroplast membrane and its ability to peroxidize di- and mono-galactolipid PUFAs (mainly MGDG/DGDG 36:6 in grapevine leaves).[23,63] As reported for other LOXs,[29] a prevalent negative charge at the interface of the PLAT/catalytic domain is present although binding of divalent (Ca^{2+}) ions mediating the interaction with the negative headgroups of phospholipids is not applicable to LoxA, which interacts with neutral galactolipids.

The canonical boot-shaped active site of plant LOXs[26] is present in LoxA with aliphatic residues along the cavity available to accommodate the substrate fatty acid chain. A phenylalanine at the bottom determines cavity depth and regio-specificity of the O_2 addition site as confirmed by product analysis of different LoxA substrates. However, active site entrance is completely blocked by a leucine pair (leucine gate, cork) from the LID and the invariant leucine from the arched helix (Leu606). In the open conformation obtained in the presence of $C_{12}E_9$, the gate is opened by LID disordering and the active site becomes solvent exposed. Moreover, due to LID melting N755 is turned away from the catalytic iron, possibly allowing O_2 addition on the 13-S site of the radical intermediate. The conformational change of the LID that activates the enzyme by opening the catalytic site entrance has been already described for specific lipases, such as *Rhizopus chinensis*, where the flipping of a Phe residue, even improved by Trp substitution, seems to be pivotal for the transition from closed to open conformation.[64]

Finally, detergent addition highlights the presence of an allosteric site at the PLAT/catalytic domain interface, accommodating the polar head of one molecule of detergent. This pocket closely resembles the 13-HpODE allosteric effector binding site described for epithelial human 15-lipoxygenase (15-hLO-2), where it affects both substrate specificity and catalytic efficiency by enhancing enzyme-substrate complex formation in the active site.[54] As observed for grapevine LoxA in the current study, the loss of the dimeric structure of h12-LOX (using a monomeric mutant) abolished the allosteric regulation of the enzyme.[58] Apparently, LoxA activity and regulation are mediated by the ability of the dimer to interact with the membrane and to dissolve the LID, thereby unmasking allosteric and catalytic sites. The correlation between conformational changes and enzymatic activity of dimeric LoxA are mirrored by tryptophan fluorescence data reinforcing a mechanism of pH dependent local rearrangements in the presence of a lipidic surface. The LoxA structure highlighted the presence of three coupled tryptophan/histidine clusters, making it difficult to correctly delineate the causality of events from the observed fluorescence behavior. The conformational changes at the PLAT/-catalytic domain interface, including W100 flipping connected with a tight histidine scaffold in PLAT, might induce the tryptophan embedding in a hydrophobic environment. This behavior resembles the trapping of the cytosolic Phospholipase A2 (cPLA2) on L-DOPM vesicles,[65] and of the human 5-LOX, for which the C2-like domain has been proposed to bind to the membrane via Ca^{2+} mediated insertion of tryptophan residues.[66,67]

Overall, our structural and functional characterization allows to devise an elegant model for LoxA catalytic activity *in vivo* (Figure 9): in the chloroplast stroma at a pH below 6.2 the LoxA dimer is in a closed conformation and behaves like a poorly active soluble enzyme. However, above pH 6.2 LoxA is able to interact with the galactolipid membrane by opening of the LID domain and anchoring to the membrane by the PLAT domain (including tryptophan W100). Anchoring is possibly enforced by an allosteric site which accommodates the polar sugar head of the MGDG. As for an interfacial enzyme, the MGDG/DGDG substrates can directly access the catalytic site from the membrane phase, avoiding solvent contact.

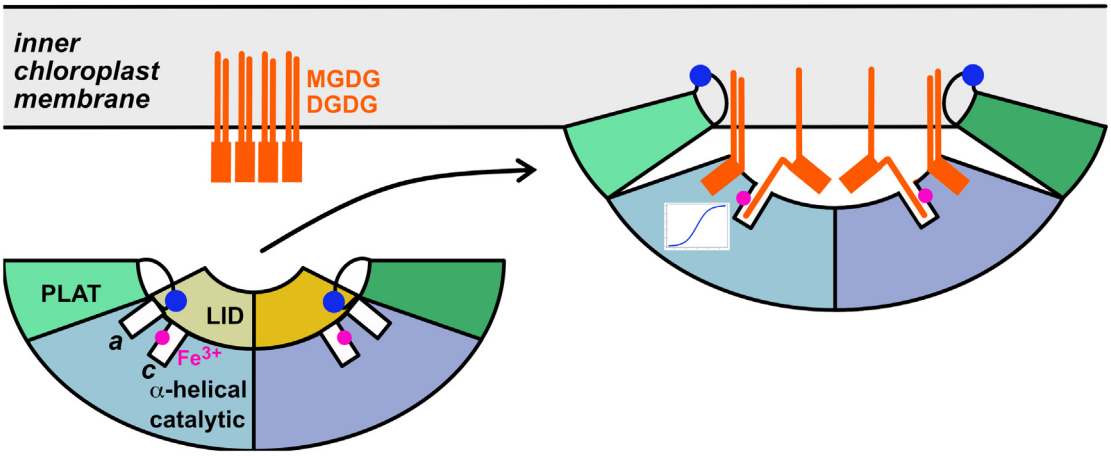

Figure 9. Model for LoxA activation at the inner chloroplast membrane. Left: Below pH 6.2, the LoxA dimer in its closed conformation behaves like a poorly active soluble enzyme. **Right:** Above pH 6.2, LoxA is able to interact with the galactolipid membrane by opening of the LID domains, anchoring by means of the PLAT domains (including tryptophan W100, blue sphere), and the allosteric site (a) which accommodates the polar sugar head of the mono- and di-galactolipids (MGDG, DGDG). As for an interfacial enzyme, the MGDG/DGDG substrates (orange) can directly access the catalytic sites (c) from the membrane phase, avoiding solvent contact. Under these conditions, a positive cooperative kinetic is observed (inset).

Our study of LoxA kinetics provided further functional information to complete this model. Firstly, enzymatic activity measured on free linolenic acid chains was improved by the addition of $C_{12}E_9$, as well as Tween20 above their CMC. Moreover, velocity was dependent on the LnA/detergent molar ratio, rather than on LnA alone, indicating that the actual substrate concentration was represented by the fraction of substrate partitioning into micelles. In other words, the enzyme shows a preference for LnA chains inserted in micellar structures. This is typical for interfacial catalysis, where enzyme activity is controlled by the concentration of substrates at interfaces.[68] The Michaelis-Menten model only applies to soluble enzymes and substrates present in the same phase. In the case of interfacial catalysis, kinetic parameters such as V_{max} and K_M, are best quantified as moles per unit area. Even though our *in vitro* system does not contain a lipidic bilayer, it mimics the *in vivo* situation and provides evidence for how the lipidic bilayer supports LoxA ability to peroxidize esterified membrane galactolipid PUFA chains.

Secondly, LoxA shows a cooperative behavior in a narrow pH interval centered at its optimal pH 6.4. At lower pH (acidic side of the activity vs. pH profile), LoxA follows a simple Michaelis-Menten kinetics, likely not interacting with the lipid moiety as also suggested by Trp fluorescence. Around pH 6.2, the protonation state of some important residues apparently changes allowing for membrane binding, LID removal, substrate entrance access, and occupancy of the allosteric site. A polar molecule, such as the galactose unit of MGDG is a likely candidate allowing for allostery with positive cooperativity. This model would classify LoxA as an interfacial enzyme with an interfacial activation mechanism according to literature[61]. The study of the monomeric mutant supports the relevance of the dimeric nature for the interaction with the membrane and cooperativity. The protonation state of one or more residues seems relevant for catalysis, explaining the steep activity decrease on the basic side of the pH profile. With pK_a values in the pH range between 6 and 7, it is tempting to propose that histidines act as pH sensors and regulators of LoxA catalysis (in the analyzed *in vitro* conditions) by being distinctly involved either in membrane binding or in catalysis. *In vivo*, the far most prevalence of 36:6 galactolipids in grapevine chloroplast membranes suggests that the enzyme works at saturating conditions and maximum rate. Together with the formation of higher LoxA oligomers, and likely a low dissociation constant typical of interfacial enzymes, we speculate that LoxA might produce hotspots of peroxidation at the chloroplast inner membrane.

Conclusions

Our study describes stable dimeric structures of the grapevine lipoxygenase LoxA defining two functionally relevant conformations, which are intimately linked to LoxA ability to interact with lipidic membranes. The transition from the closed to open conformation involves the removal of a LID domain on each monomer, which renders the active site and an allosteric site solvent accessible and confer LoxA the ability to peroxidize membrane lipids with positive cooperativity. The mechanism of interfacial activation and catalysis is not shared by all grapevine LOX enzymes, but is likely conserved for specific isoforms also in other organisms.

Author contribution statement

S.P., **C.M.** and **I.S.** designed the study; **A.G.** and **I.H.** purified and crystallized proteins, and solved the X-ray structures; **Y.H.** produced and analyzed the LoxA double mutant; **K.W.** built and analyzed the structures; **S.P.** perfomed activity assays and SEC analysis; **M.D.S.** performed Trp fluorescence analysis; **G.G.** perfomed HPLC-MS/MS analysis of reaction products; **S.P., K.W., C.M.** and **I.S.** analyzed the data and wrote the manuscript.

Funding information

This work was supported by the DFG (Deutsche Forschungsgemeinschaft) through the Leibniz Programme (SI 586/6-1) and TRR83 (TP22) to I. S., and by the Autonomous Province of Trento (PAT-ADP 2017-2019) to C.M..

CRediT authorship contribution statement

Stefania Pilati: Writing – original draft, Investigation, Formal analysis, Conceptualization. **Klemens Wild:** Writing – original draft, Visualization, Formal analysis, Data curation. **Andrea Gumiero:** Investigation, Formal analysis. **Iris Holdermann:** Investigation, Formal analysis. **Yvonne Hackmann:** Investigation, Formal analysis. **Mauro Dalla Serra:** Supervision, Investigation, Formal analysis. **Graziano Guella:** Supervision, Investigation, Formal analysis. **Claudio Moser:** Writing – review & editing, Supervision, Funding acquisition, Conceptualization. **Irmgard Sinning:** Writing – review & editing, Formal analysis, Supervision, Funding acquisition, Conceptualization.

DATA AVAILABILITY

The atomic coordinates and structure factors of LoxA from grapevine have been deposited in the Protein Data Bank (PDB) with entry IDs: **8QDQ** for the closed conformation and **8QDR** for the open conformation.

DECLARATION OF COMPETING INTEREST

The authors declare that they have no known competing financial interests or personal relationships that could have appeared to influence the work reported in this paper.

Acknowledgements

We would like to dedicate this work to the memory of **Claudio Moser**, who recently passed away still young, and thank him for his constant encouragement, support and friendship. We thank Franco Biasioli for statistical support with R, Daniela Bertoldi for metal-bound analysis by ICP at Fondazione E. Mach, Adriano Sterni at University of Trento and Marta Marchioretto at CNR for technical support, Claudia Siegmann and Jürgen Kopp from the BZH/CellNetworks crystallization platform for protein crystallization, and acknowledge excellent technical support by Astrid Hendricks. We acknowledge access to the European Synchrotron Radiation Facility (ESRF) beamlines ID23-1, ID29 and BM29. We acknowledge the data storage service SDS@hd and bwHPC supported by the Ministry of Science, Research and the Arts Baden-Württemberg (MWK) and the Deutsche Forschungsgemeinschaft (DFG) through grants INST 35/1314-1 FUGG and INST 35/1134-1 FUGG.

Appendix A. Supplementary material

Supplementary material to this article can be found online at https://doi.org/10.1016/j.jmb.2024.168821.

Received 17 July 2024;
Accepted 12 October 2024;
Available online 17 October 2024

Keywords:
Vitis vinifera (grapevine);
lipoxygenase (LOX);
crystal structure;
lipid peroxidation;
allosteric enzyme;
interfacial activation

Abbreviations13-LOX, 13S-lipoxygenase; LnA, α-linolenic acid; 13-HODE, 13(S)-hydroxyoctadeca-9Z,11E-dienoic acid; 13-HOTrE, 13(S)-hydroxyoctadeca-9Z,11E,15Z-trienoic acid; PUFA, poly unsaturated fatty acid; MGDG, monogalactosyl diacyl-glycerol; DGDG, digalactosyl diacyl-glycerol; SAXS, small angle X-ray scattering; MALS, multiangle light scattering; CMC, critical micellar concentration

References

1. Liavonchanka, A., Feussner, I., (2006). Lipoxygenases: Occurrence, functions and catalysis. *J. Plant Physiol.* **163**, 348–357. https://doi.org/10.1016/j.jplph.2005.11.006.
2. Andreou, A., Feussner, I., (2009). Lipoxygenases–structure and reaction mechanism. *Phytochemistry* **70**, 1504–1510. https://doi.org/10.1016/j.phytochem.2009.05.008.
3. Tolley, J.P., Nagashima, Y., Gorman, Z., Kolomiets, M.V., Koiwa, H., (2018). Isoform-specific subcellular localization of Zea mays lipoxygenases and oxo-phytodienoate reductase 2, Plant. *Gene* **13**, 36–41. https://doi.org/10.1016/j.plgene.2017.12.002.

4. Camargo, P.O., Calzado, N.F., Budzinski, I.G.F., Domingues, D.S., (2023). Genome-wide analysis of lipoxygenase (LOX) genes in angiosperms. *Plants* **12** https://doi.org/10.3390/plants12020398.
5. Brash, A.R., (1999). Lipoxygenases: occurrence, functions, catalysis, and acquisition of substrate. *J. Biol. Chem.* **274**, 23679–23682. https://doi.org/10.1074/JBC.274.34.23679.
6. Mosblech, A., Feussner, I., Heilmann, I., (2009). Oxylipins: structurally diverse metabolites from fatty acid oxidation. *Plant Physiol Biochem. J.* **47**, 511–517. https://doi.org/10.1016/j.plaphy.2008.12.011.
7. Farmer, E.E., Mueller, M.J., (2013). ROS-mediated lipid peroxidation and RES-activated signaling. *Annu. Rev. Plant Biol.* **64**, 429–450. https://doi.org/10.1146/annurev-arplant-050312-120132.
8. Matsui, K., Engelberth, J., (2022). Green leaf volatiles – the forefront of plant responses against biotic attack. *Plant Cell Physiol.* **63**, 1378–1390. https://doi.org/10.1093/pcp/pcac117.
9. Shen, J., Tieman, D., Jones, J.B., Taylor, M.G., Schmelz, E., Huffaker, A., Bies, D., Chen, K., Klee, H.J., (2014). A 13-lipoxygenase, TomloxC, is essential for synthesis of C5 flavour volatiles in tomato. *J. Exp. Bot.* **65**, 419–428. https://doi.org/10.1093/jxb/ert382.
10. Bhowmik, P., Yan, W., Hodgins, C., Polley, B., Warkentin, T., Nickerson, M., Ro, D.K., Marsolais, F., Domoney, C., Shariati-Ievari, S., Aliani, M., (2023). CRISPR/Cas9-mediated lipoxygenase gene-editing in yellow pea leads to major changes in fatty acid and flavor profiles. *Front. Plant Sci.* **14** https://doi.org/10.3389/fpls.2023.1246905.
11. Loeffler, C., Berger, S., Guy, A., Durand, T., Bringmann, G., Dreyer, M., Von Rad, U., Durner, J., Mueller, M.J., (2005). B1-phytoprostanes trigger plant defense and detoxification responses. *Plant Physiol.* **137**, 328–340. https://doi.org/10.1104/pp.104.051714.
12. Christensen, S.A., Huffaker, A., Kaplan, F., Sims, J., Ziemann, S., Doehlemann, G., Ji, L., Schmitz, R.J., Kolomiets, M.V., Alborn, H.T., Mori, N., Jander, G., Ni, X., Sartor, R.C., Byers, S., Abdo, Z., Schmelz, E.A., (2015). Maize death acids, 9-lipoxygenase-derived cyclopente(a)nones, display activity as cytotoxic phytoalexins and transcriptional mediators. *Proc. Natl. Acad. Sci. U. S. A.* **112**, 11407–11412. https://doi.org/10.1073/pnas.1511131112.
13. Zoeller, M., Stingl, N., Krischke, M., Fekete, A., Waller, F., Berger, S., Mueller, M.J., (2012). Lipid profiling of the Arabidopsis hypersensitive response reveals specific lipid peroxidation and fragmentation processes: Biogenesis of pimelic and azelaic acid. *Plant Physiol.* **160**, 365–378. https://doi.org/10.1104/pp.112.202846.
14. Feussner, I., Wasternack, C., Kindl, H., Kühn, H., (1995). Lipoxygenase-catalyzed oxygenation of storage lipids is implicated in lipid mobilization during germination. *Proc. Natl. Acad. Sci. U. S. A.* **92**, 11849–11853. https://doi.org/10.1073/pnas.92.25.11849.
15. Springer, A., Kang, C., Rustgi, S., von Wettstein, D., Reinbothe, C., Pollmann, S., Reinbothe, S., (2016). Programmed chloroplast destruction during leaf senescence involves 13-lipoxygenase (13-LOX). *Proc. Natl. Acad. Sci. U. S. A.* **113**, 3383–3388. https://doi.org/10.1073/pnas.1525747113.
16. Ding, Y., Yang, W., Su, C., Ma, H., Pan, Y., Zhang, X., Li, J., (2019). Tandem 13-lipoxygenase genes in a cluster confers yellow-green leaf in cucumber. *Int. J. Mol. Sci.* **20** https://doi.org/10.3390/ijms20123102.
17. Kanofskysb, J.R., Axelrod, B., (1986). Singlet oxygen production by soybean lipoxygenase isozymes. *J. Biol. Chem.* **261**, 1099–1104 https://www.jbc.org/article/S0021-9258(17)36059-3/pdf.
18. Birtic, S., Ksas, B., Genty, B., Mueller, M.J., Triantaphylidès, C., Havaux, M., (2011). Using spontaneous photon emission to image lipid oxidation patterns in plant tissues. *Plant J.* **67**, 1103–1115. https://doi.org/10.1111/j.1365-313X.2011.04646.x.
19. Prasad, A., Ferretti, U., Sedlářová, M., Pospíšil, P., (2016). Singlet oxygen production in Chlamydomonas reinhardtii under heat stress. *Sci. Rep.* **6**, 20094. https://doi.org/10.1038/srep20094.
20. Prasad, A., Sedlářová, M., Kale, R.S., Pospíšil, P., (2017). Lipoxygenase in singlet oxygen generation as a response to wounding: *In vivo* imaging in Arabidopsis thaliana. *Sci. Rep.* **7**, 9831. https://doi.org/10.1038/s41598-017-09758-1.
21. Chen, T., Cohen, D., Itkin, M., Malitsky, S., Fluhr, R., (2021). Lipoxygenase functions in $^1O_2$ production during root responses to osmotic stress. *Plant Physiol.* **185**, 1638–1651. https://doi.org/10.1093/plphys/kiab025.
22. Negri, A.S., Robotti, E., Prinsi, B., Espen, L., Marengo, E., (2011). Proteins involved in biotic and abiotic stress responses as the most significant biomarkers in the ripening of Pinot Noir skins, Funct. Integr. *Genomics* **11**, 341–355. https://doi.org/10.1007/s10142-010-0205-0.
23. Pilati, S., Brazzale, D., Guella, G., Milli, A., Ruberti, C., Biasioli, F., Zottini, M., Moser, C., (2014). The onset of grapevine berry ripening is characterized by ROS accumulation and lipoxygenase-mediated membrane peroxidation in the skin. *BMC Plant Biol.* **14**, 87. https://doi.org/10.1186/1471-2229-14-87.
24. Pilati, S., Bagagli, G., Sonego, P., Moretto, M., Brazzale, D., Castorina, G., Simoni, L., Tonelli, C., Guella, G., Engelen, K., Galbiati, M., Moser, C., (2017). Abscisic acid is a major regulator of grape berry ripening onset: New insights into ABA signaling network. *Front. Plant Sci.* **8**, 1093. https://doi.org/10.3389/fpls.2017.01093.
25. Newie, J., Andreou, A., Neumann, P., Einsle, O., Feussner, I., Ficner, R., (2016). Crystal structure of a lipoxygenase from *Cyanothece* sp. may reveal novel features for substrate acquisition. *J. Lipid Res.* **57**, 276–287. https://doi.org/10.1194/jlr.M064980 (accessed March 27, 2017).
26. Neau, D.B., Bender, G., Boeglin, W.E., Bartlett, S.G., Brash, A.R., Newcomer, M.E., (2014). Crystal structure of a lipoxygenase in complex with substrate: the arachidonic acid-binding site of 8R-lipoxygenase. *J. Biol. Chem.* **289**, 31905–31913. https://doi.org/10.1074/jbc.M114.599662.
27. Zaragoza, J.P.T., Offenbacher, A.R., Hu, S., Gee, C.L., Firestein, Z.M., Minnetian, N., Deng, Z., Fan, F., Iavarone, A.T., Klinman, J.P., (2023). Temporal and spatial resolution of distal protein motions that activate hydrogen tunneling in soybean lipoxygenase. *Proc. Natl. Acad. Sci.* **120**, https://doi.org/10.1073/pnas.2211630120 e2211630120.
28. Garreta, A., Val-Moraes, S.P., García-Fernández, Q., Busquets, M., Juan, C., Oliver, A., Ortiz, A., Gaffney, B. J., Fita, I., Manresa, À., Carpena, X., (2013). Structure and interaction with phospholipids of a prokaryotic lipoxygenase from *Pseudomonas aeruginosa*. *FASEB J.* **27**, 4811–4821. https://doi.org/10.1096/fj.13-235952.
29. Droege, K.D., Keithly, M.E., Sanders, C.R., Armstrong, R. N., Thompson, M.K., (2017). Structural dynamics of 15-

lipoxygenase-2 via hydrogen-deuterium exchange. *Biochemistry* **56**, 5065–5074. https://doi.org/10.1021/acs.biochem.7b00559.
30. Winter, G., (2010). Xia2: An expert system for macromolecular crystallography data reduction. *J. Appl. Crystallogr.* **43**, 186–190. https://doi.org/10.1107/S0021889809045701.
31. Evans, P.R., Murshudov, G.N., (2013). How good are my data and what is the resolution? *Acta Crystallogr. Sect. D Biol. Crystallogr.* **69**, 1204–1214. https://doi.org/10.1107/S0907444913000061.
32. Liebschner, D., Afonine, P.V., Baker, M.L., Bunkoczi, G., Chen, V.B., Croll, T.I., Hintze, B., Hung, L.W., Jain, S., McCoy, A.J., Moriarty, N.W., Oeffner, R.D., Poon, B.K., Prisant, M.G., Read, R.J., Richardson, J.S., Richardson, D. C., Sammito, M.D., Sobolev, O.V., Stockwell, D.H., Terwilliger, T.C., Urzhumtsev, A.G., Videau, L.L., Williams, C.J., Adams, P.D., (2019). Macromolecular structure determination using X-rays, neutrons and electrons: Recent developments in Phenix. *Acta Crystallogr. Sect. D Struct. Biol.* **75**, 861–877. https://doi.org/10.1107/S2059798319011471.
33. Emsley, P., Lohkamp, B., Scott, W.G., Cowtan, K., (2010). Features and development of Coot. *Acta Crystallogr. Sect. D Biol. Crystallogr.* **66**, 486–501. https://doi.org/10.1107/S0907444910007493.
34. Williams, C.J., Headd, J.J., Moriarty, N.W., Prisant, M.G., Videau, L.L., Deis, L.N., Verma, V., Keedy, D.A., Hintze, B. J., Chen, V.B., Jain, S., Lewis, S.M., Arendall, W.B., Snoeyink, J., Adams, P.D., Lovell, S.C., Richardson, J.S., Richardson, D.C., (2018). MolProbity: More and better reference data for improved all-atom structure validation. *Protein Sci.* **27**, 293–315. https://doi.org/10.1002/pro.3330.
35. Franke, D., Petoukhov, M.V., Konarev, P.V., Panjkovich, A., Tuukkanen, A., Mertens, H.D.T., Kikhney, A.G., Hajizadeh, N.R., Franklin, J.M., Jeffries, C.M., Svergun, D.I., (2017). ATSAS 2.8: A comprehensive data analysis suite for small-angle scattering from macromolecular solutions. *J. Appl. Crystallogr.* **50**, 1212–1225. https://doi.org/10.1107/S1600576717007786.
36. Konarev, P.V., Volkov, V.V., Sokolova, A.V., Koch, M.H.J., Svergun, D.I., (2003). PRIMUS: A Windows PC-based system for small-angle scattering data analysis. *J. Appl. Crystallogr.* **36**, 1277–1282. https://doi.org/10.1107/S0021889803012779.
37. Franke, D., Svergun, D.I., (2009). DAMMIF, a program for rapid ab-initio shape determination in small-angle scattering. *J. Appl. Crystallogr.* **42**, 342–346. https://doi.org/10.1107/S0021889809000338.
38. Axelrod, B., Cheesbrough, T.M., Laakso, S., (1981). [53] Lipoxygenase from soybeans. *Methods Enzymol.* **71**, 441–451. https://doi.org/10.1016/0076-6879(81)71055-3.
39. Helenius, A., McCaslin, D.R., Fries, E., Tanford, C., (1979). Properties of detergents. *Methods Enzymol.* **56**, 734–749. https://doi.org/10.1016/0076-6879(79)56066-2.
40. R Core Team (2024). R: A Language and Environment for Statistical Computing. https://www.r-project.org/.
41. Ivanov, I., Shang, W., Toledo, L., Masgrau, L., Svergun, D. I., Stehling, S., Gómez, H., Di Venere, A., Mei, G., Lluch, J. M., Skrzypczak-Jankun, E., González-Lafont, À., Kühn, H., (2012). Ligand-induced formation of transient dimers of mammalian 12/15-lipoxygenase: A key to allosteric behavior of this class of enzymes? *Proteins Struct. Funct. Bioinforma.* **80**, 703–712. https://doi.org/10.1002/prot.23227.
42. Krissinel, E., Henrick, K., (2007). Inference of Macromolecular Assemblies from Crystalline State. *J. Mol. Biol.* **372**, 774–797. https://doi.org/10.1016/j.jmb.2007.05.022.
43. Bateman, A., Sandford, R., (1999). The PLAT domain: a new piece in the PKD1 puzzle. *Curr. Biol.* **9**, R588–R590. https://doi.org/10.1016/s0960-9822(99)80380-7.
44. Offenbacher, A.R., Holman, T.R., (2020). Fatty acid allosteric regulation of C-H activation in plant and animal lipoxygenases. *Molecules* **25**, 3374. https://doi.org/10.3390/molecules25153374.
45. Walther, M., Wiesner, R., Kuhn, H., (2004). Investigations into calcium-dependent membrane association of 15-lipoxygenase-1: Mechanistic roles of surface-exposed hydrophobic amino acids and calcium. *J. Biol. Chem.* **279**, 3717–3725. https://doi.org/10.1074/jbc.M309564200.
46. Boyington, J.C., Gaffney, B.J., Amzel, L.M., (1993). The three-dimensional structure of an arachidonic acid 15-lipoxygenase. *Science (80-)* **260**, 1482–1486. https://doi.org/10.1126/science.8502991.
47. Newcomer, M.E., Brash, A.R., (2015). The structural basis for specificity in lipoxygenase catalysis. *Protein Sci.* **24**, 298–309. https://doi.org/10.1002/pro.2626.
48. Eek, P., Järving, R., Järving, I., Gilbert, N.C., Newcomer, M.E., Samel, N., (2012). Structure of a calcium-dependent 11R-lipoxygenase suggests a mechanism for Ca^{2+} regulation. *J. Biol. Chem.* **287**, 22377–22386. https://doi.org/10.1074/jbc.M112.343285.
49. Minor, W., Steczko, J., Stec, B., Otwinowski, Z., Bolin, J.T., Walter, R., Axelrod, B., (1996). Crystal structure of soybean lipoxygenase L-1 at 1.4 Å resolution. *Biochemistry* **35**, 10687–10701. https://doi.org/10.1021/bi960576u.
50. Haglid, K.G., Hamberger, A., Hansson, H.A., HydéN, H., Persson, L., Rönnbäck, L., (1975). Letters to nature. *Nature* **258**, 748–749. https://doi.org/10.1038/258748a0.
51. Coffa, G., Imber, A.N., Maguire, B.C., Laxmikanthan, G., Schneider, C., Gaffney, B.J., Brash, A.R., (2005). On the relationships of substrate orientation, hydrogen abstraction, and product stereochemistry in single and double dioxygenations by soybean lipoxygenase-1 and its Ala542Gly mutant. *J. Biol. Chem.* **280**, 38756–38766. https://doi.org/10.1074/jbc.M504870200.
52. Xu, S., Mueser, T.C., Marnett, L.J., Funk, M.O., (2012). Crystal structure of 12-Lipoxygenase catalytic-domain-inhibitor complex identifies a substrate-binding channel for catalysis. *Structure* **20**, 1490–1497. https://doi.org/10.1016/j.str.2012.06.003.
53. Gaffney, B.J., (2020). EPR spectroscopic studies of lipoxygenases. *Chem. – Asian J.* **15**, 42–50. https://doi.org/10.1002/asia.201901461.
54. Wecksler, A.T., Kenyon, V., Garcia, N.K., Deschamps, J. D., Van Der Donk, W.A., Holman, T.R., (2009). Kinetic and structural investigations of the allosteric site in human epithelial 15-lipoxygenase-2. *Biochemistry* **48**, 8721–8730. https://doi.org/10.1021/bi9009242.
55. Podolyan, A., White, J., Jordan, B., Winefield, C., (2010). Identification of the lipoxygenase gene family from Vitis vinifera and biochemical characterisation of two 13-lipoxygenases expressed in grape berries of Sauvignon Blanc. *Funct. Plant Biol.* **37**, 767–784. https://doi.org/10.1071/FP09271.

56. Choi, J., Chon, J., Kim, S., Shin, W., (2008). Conformational flexibility in mammalian 15S-lipoxygenase: Reinterpretation of the crystallographic data. *Proteins* **70**, 1023–1032. https://doi.org/10.1002/prot.21590.
57. Di Venere, A., Nicolai, E., Ivanov, I., Dainese, E., Adel, S., Angelucci, B.C., Kuhn, H., Maccarrone, M., Mei, G., (2014). Probing conformational changes in lipoxygenases upon membrane binding: Fine-tuning by the active site inhibitor ETYA. *Biochim. Biophys. Acta – Mol. Cell Biol. Lipids.* **1841**, 1–10. https://doi.org/10.1016/j.bbalip.2013.08.015.
58. Tsai, W.C., Aleem, A.M., Whittington, C., Cortopassi, W.A., Kalyanaraman, C., Baroz, A., Iavarone, A.T., Skrzypczak-Jankun, E., Jacobson, M.P., Offenbacher, A.R., Holman, T., (2021). Mutagenesis, hydrogen-deuterium exchange, and molecular docking investigations establish the dimeric interface of human platelet-type 12-lipoxygenase. *Biochemistry* **60**, 802–812. https://doi.org/10.1021/acs.biochem.1c00053.
59. Mobbs, J.I., Black, K.A., Tran, M., Burger, W.A.C., Venugopal, H., Holman, T.R., Holinstat, M., Thal, D., Glukhova, A., (2023). Cryo-EM structures of human arachidonate 12S-Lipoxygenase (12-LOX) bound to endogenous and exogenous inhibitors. *Blood J.* **142**, 1233–1242. https://doi.org/10.1182/blood.2023020441.
60. Gillmor, S.A., Villaseñor, A., Fletterick, R., Sigal, E., Browner, M.F., (1997). The structure of mammalian 15-lipoxygenase reveals similarity to the lipases and the determinants of substrate specificity. *Nature Struct. Biol.* **4**, 1003–1009. https://doi.org/10.1038/nsb1297-1003.
61. Gelb, M.H., Min, J.H., Jain, M.K., (2000). Do membrane-bound enzymes access their substrates from the membrane or aqueous phase: Interfacial versus non-interfacial enzymes. *Biochim. Biophys. Acta – Mol. Cell Biol. Lipids.* **1488**, 20–27. https://doi.org/10.1016/S1388-1981(00)00106-2.
62. Winget, J.M., Pan, Y.H., Bahnson, B.J., (2006). The interfacial binding surface of phospholipase A2s. *Biochim. Biophys. Acta – Mol. Cell Biol. Lipids.* **1761**, 1260–1269. https://doi.org/10.1016/j.bbalip.2006.08.002.
63. Masuero, D., Škrab, D., Chitarrini, G., Garcia-aloy, M., Franceschi, P., Sivilotti, P., Guella, G., Vrhovsek, U., (2021). Grape lipidomics: An extensive profiling thorough uhplc–ms/ms method. *Metabolites* **11**, 827. https://doi.org/10.3390/metabo11120827.
64. Wang, S., Xu, Y., Yu, X.W., (2021). A phenylalanine dynamic switch controls the interfacial activation of Rhizopus chinensis lipase. *Int. J. Biol. Macromol.* **173**, 1–12. https://doi.org/10.1016/j.ijbiomac.2021.01.086.
65. Bayburt, T., Gelb, M.H., (1997). Interfacial catalysis by human 85 kDa cytosolic phospholipase A2 on anionic vesicles in the scooting mode. *Biochemistry* **36**, 3216–3231. https://doi.org/10.1021/bi961659d.
66. Kulkarni, S., Das, S., Funk, C.D., Murray, D., Cho, W., (2002). Molecular basis of the specific subcellular localization of the C2-like domain of 5-lipoxygenase. *J. Biol. Chem.* **277**, 13167–13174. https://doi.org/10.1074/jbc.M112393200.
67. Radmark, O., Samuelsson, B., (2009). 5-Lipoxygenase: Mechanisms of regulation. *J. Lipid Res.* **50**, S40. https://doi.org/10.1194/jlr.R800062-JLR200.
68. Reis, P., Holmberg, K., Watzke, H., Leser, M.E., Miller, R., (2009). Lipases at interfaces: A review. *Adv. Colloid Interface Sci.* **147–148**, 237–250. https://doi.org/10.1016/j.cis.2008.06.001.